Heliyon 7 (2021) e06654

Contents lists available at ScienceDirect

Heliyon

journal homepage: www.cell.com/heliyon

Research article

Synthesis and characterization of coal fly ash and palm oil fuel ash modified artisanal and small-scale gold mine (ASGM) tailings based geopolymer using sugar mill lime sludge as Ca-based activator

Einstine M. Opiso [a,*], Carlito B. Tabelin [b], Christian V. Maestre [c], John Paul J. Aseniero [c], Ilhwan Park [d], Mylah Villacorte-Tabelin [e]

[a] Geo-environmental Engineering Group, Civil Engineering Department, Central Mindanao University, Bukidnon, Philippines
[b] School of Minerals and Energy Resources Engineering, The University of New South Wales, Sydney, NSW, Australia
[c] Materials Science Research Group, Physics Department, Central Mindanao University, Bukidnon, Philippines
[d] Division of Sustainable Resources Engineering, Faculty of Engineering, Hokkaido University, Sapporo, Japan
[e] Department of Biological Sciences, College of Science and Mathematics, Mindanao State University–Iligan Institute of Technology, Iligan City, Philippines

ARTICLE INFO

Keywords:
Geopolymerization
Mine tailings
Sugar mill lime sludge
Fly ash
Palm oil fuel ash
Powder activator

ABSTRACT

The continuous accumulation of artisanal and small-scale gold mining (ASGM) tailings in the Philippines without adequate storage and disposal facility could lead to human health and environmental disasters in the long run. In this study, ASGM tailings was simultaneously stabilized and repurposed as construction material via geopolymerization using coal fly ash, palm oil fuel ash and a powder-based alkali activator. Scanning electron microscopy with energy dispersive X-ray spectroscopy (SEM-EDS) identified iron sulfides in the tailings containing arsenic (As), cadmium (Cd), copper (Cu), lead (Pb) and zinc (Zn), which could be released via weathering. The average unconfined compressive strengths (UCS) of tailings-based geopolymers at 14 days curing were 7.58 MPa and 7.7 MPa with fly ash and palm oil fuel ash, respectively. The tailings-based geopolymers with palm oil fuel ash had higher UCS most likely due to CASH reaction product formation that improved strength formation. The toxicity characteristic leaching procedure (TCLP) results showed very low leachabilities of As, Pb and Fe in the geopolymer materials suggesting ASGM tailings was effectively encapsulated within the geopolymer matrix. Overall, the geopolymerization of ASGM tailings is a viable and promising solution to simultaneously stabilize mining and industrial wastes and repurpose them into construction materials.

1. Introduction

Gold (Au) is one of the most valuable metals known to man. Traditionally, this metal is extensively used in jewellery and as a safe investment in the banking and financial sectors (Calderon et al., 2019, 2020; Jeon et al., 2020a, b) but in recent years, it is finding a myriad of other rapidly growing applications like (i) corrosion-resistant wires and coatings in integrated circuits and printed circuit boards for electronics, computers and high-tech gadgets (Phengsaart et al., 2018; Jeon et al., 2018a, b, 2019), (ii) as catalysts in electric cars and clean technologies (Ghenciu, 2002; Zielasek et al., 2006), (iii) as detectors in ultra-sensitive sensors (Löfås and Johnsson, 1990; Lucarelli et al., 2004), and (iv) as a promising drug delivery system for cancer research (Ghosh et al., 2008; Paciotti et al., 2004). Because of its versatility, Au price has rapidly increased in the last 20 years fueling high demand for this precious metal worldwide (Huang and Kilic, 2019).

Large-scale mining operations employing state-of-the-art Au hydrometallurgical techniques and following strict environmental and waste management protocols are the norm worldwide (Tabelin et al., 2021), but small-scale gold mining (ASGM) operations remain commonplace especially in low- and middle-income countries. In 2011, for example, Velásquez-López et al. (2011) estimated about 15 million active ASGM operations in over 70 countries. The ASGM industry still heavily rely on gravity separation-amalgamation, a primitive approach wherein fine particles of "free" Au are concentrated using panning followed by the addition of mercury to form a gold-mercury amalgam, which is then retorted to remove mercury via volatilization. This rudimentary technique is not only inefficient in terms of Au recovery but also potentially

* Corresponding author.
E-mail address: einstineopiso@cmu.edu.ph (E.M. Opiso).

https://doi.org/10.1016/j.heliyon.2021.e06654
Received 15 April 2020; Received in revised form 29 June 2020; Accepted 29 March 2021

disastrous to the health of miners as well as the surrounding environment because processing wastewater and tailings from the majority of ASGM operations are simply discarded without treatment (Aseniero et al., 2019; Tabelin et al., 2020a). This means that excess mercury could easily find its way to rivers, water bodies and bioaccumulate in the food web (Opiso et al., 2018; Williams et al., 1995). To make matters worse, many Au deposits mined by ASGM operations are formed under hydrothermal conditions, well-known ore-forming geological phenomena that concentrate Au and base metals like copper (Cu), lead (Pb) and zinc (Zn) in sulfide minerals like pyrite (FeS_2), chalcopyrite ($CuFeS_2$) and arsenopyrite (FeAsS) (Park et al., 2018a; Tabelin et al., 2012a, b). Upon exposure to the environment, sulfide minerals are dissolved via a combination of chemical-electrochemical reactions that are promoted by microorganisms (Li et al., 2019a, b; Seng et al., 2019a, b; Tabelin et al., 2017a, 2020b), a process that generates acidic and highly contaminated leachates containing toxic metalloids like arsenic (As) and selenium (Se) (Marove et al., 2020; Tabelin and Igarashi, 2009; Tabelin et al., 2012c, 2017b; Tamoto et al., 2015) and hazardous heavy metals like Cu and Zn (Igarashi et al., 2020; Senoro et al., 2020; Tabelin et al., 2013; Tatsuhara et al., 2012; Tomiyama et al., 2019, 2020).

Like many developing countries with rich metal and mineral resources, the Philippines has numerous ASGM operators, which accounted for almost 63% of the entire country's Au production between 2005 and 2014 (Aseniero et al., 2019). ASGM operators recover Au from the ore via amalgamation and tailings from this process are further reprocessed by cyanidation to recover more Au as shown in Figure 1(a). This "two-stage" process is also widely used in other developing countries as reported by Veiga et al. (2014), producing final tailings with mercury-cyanide complexes. The primary health and environmental problem associated with ASGM operations are due to their extensive use of mercury, which although already outlawed by the Philippine government, is still used by ASGM operators all over the country (Appleton et al., 1999, 2006; Opiso et al., 2018). The accumulation of potentially hazardous tailings is another rapidly growing environmental and human health hazard around ASGM sites. Moreover, the tailings from ASGM operations in the Philippines are poorly characterized, so whether they contain other hazardous and toxic elements besides mercury is unknown. These ASGM tailings are currently dumped into poorly designed tailings dams, stockpiled without proper containment facilities or disposed of directly to nearby streams and open fields (Opiso et al., 2018). These practices are

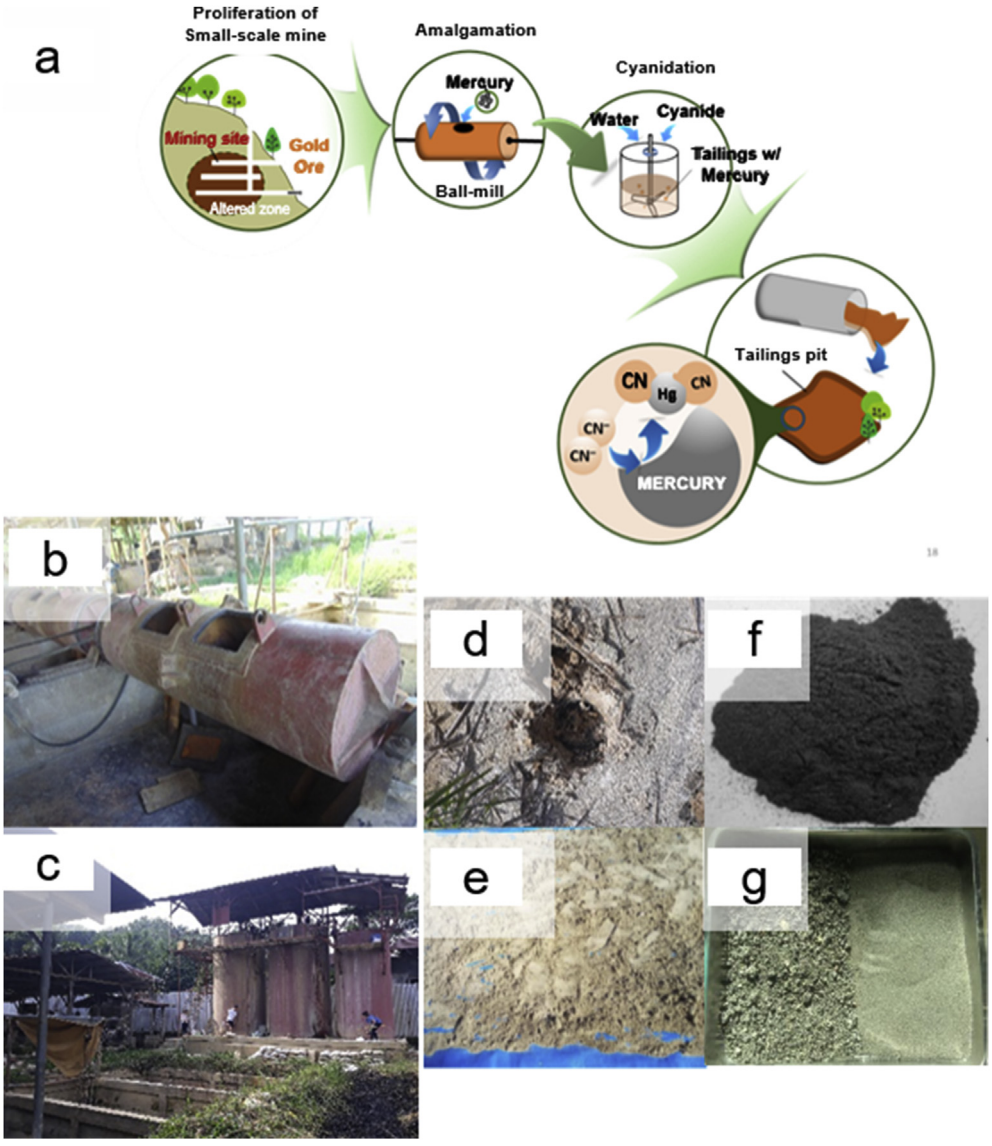

Figure 1. (a) Recovery process of gold employed by the ASGM operators and the small scale gold mine in Rosario, Agusan del Sur (b, for the ball-mill and c for the CIP plant) and the collected (d) gold mine tailings, (e) sugar mill lime sludge, (f) coal fly ash and (g) palm oil fuel ash.

exposing the surrounding communities to hazardous wastes that could cause short- and long-term negative effects to human health and the environment (Ahmari and Zhang, 2013). For example, the prevalence of mercury poisoning in communities living close to ASGM sites in Apokon, Tagum, Davao del Norte, Philippines was already reported in the studies of Appleton et al. (2006) and Akagi et al. (2000). Because of this, it is imperative to develop strategies that would stabilize or solidify tailings from ASGM operations and limit the release of toxic and hazardous contaminants into the environment.

There are numerous stabilization techniques for mine tailings such as incorporating them into a lime-cement mixture as sub-grade material (Ojuri et al., 2016; Park et al., 2019), synthesis of ceramisite (Yang et al., 2017) and phytoremediation (Wang et al., 2017), but all of them are ideal for tailings containing minute amounts of sulfide minerals. This is because sulfide minerals in tailings generate strongly acidic leachates and anions that rapidly deteriorate cement-based materials (Park et al., 2021; Tabelin et al., 2018). One recently promising approach to simultaneously repurpose and treat mine waste and tailings is via alkali activation in a process called geopolymerization. Some mine tailings are ideal geopolymer materials because they contain high clay and aluminosilicate minerals (Aseniero et al., 2019; Gitari et al., 2017), which are essential components for the geopolymer matrix to form. In this process, aluminosilicates are dissolved in highly-concentrated alkali hydroxide or silicate solution to form a structurally stable material composed of amorphous, interconnected Si–O–Al polymeric matrices via a combination of diffusion, coagulation and polycondensation (Abdel-Gawwad and Abo-El-Enein, 2016; Rajamane et al., 2009). Geopolymers have excellent mechanical properties that are sometimes comparable to concrete or fired bricks when prepared under optimum conditions (Abdul Rahim et al., 2015; Caballero et al., 2014).

A previous study of the authors reported that mine wastes and tailings from key ASGM areas in Mindanao, Philippines, contain substantial amounts of aluminosilicate and clay minerals, which make them potentially good materials for geopolymerization (Aseniero et al., 2019). Moreover, these wastes have fine particles that are known to improve the strength development of concrete (Opiso et al., 2017). However, one drawback of direct Au mine tailings activation with sodium hydroxide (NaOH) was the low compressive strength of products because of the tailings' highly variable Si-to-Al ratio, a critical parameter for optimum geopolymerization conditions (Davidovits et al., 2013; Kiventera et al., 2016; Luukkonen et al., 2017).

Another serious drawback of the conventional geopolymer activation approach is the use of strongly alkaline NaOH and sodium silicate (Na_2SiO_3) solutions. Aqueous alkali activators are difficult to handle, transport and store especially in large-scale application because they are strongly corrosive (Bayuaji et al., 2017). A workaround to this problems associated with aqueous activator usage in geopolymerization is to utilize dry, solid activators. Solid activators like solid NaOH, Na_2SiO_3, $Na_2SiO_3{\cdot}5H_2O$, Na_2CO_3, $NaAlO_2$, $CaSO_4$, Na_2SO_4, KOH, red mud, CaO, MgO, dolomite ($CaMg(CO_3)_2$), and $Ca(OH)_2$ have been employed successfully in one-part geopolymer mixes (Luukkonen et al., 2017). Among them, Ca-based solid activators are more efficient because they supply alkaline earth cations, which promote the formation of different binding phases (Li et al., 2010). Abdel-Gawwad and Abo-El-Enein (2016), for example, synthesized a dry activator composed of sodium carbonate (Na_2CO_3) and calcium hydroxide ($Ca(OH)_2$) from NaOH and $CaCO_3$, which increased the mechanical properties of the resulting geopolymer concrete.

In Mindanao, Philippines, there is a potentially good Ca-rich waste material locally available called sugar-mill lime sludge, an industrial by-product in the manufacture and refining of sugar from sugarcane, which may contain up to 80% of Ca in the form of lime (Opiso et al., 2017). Excessive $Ca(OH)_2$ in the raw material is, however, detrimental to the final geopolymer product properties because $Ca(OH)_2$ increases the relative abundance of acid-soluble C–S–H gel products (Khater, 2012). One way to inhibit the negative effects on geopolymerization of excessive $Ca(OH)_2$ is to integrate high Si- and Al-bearing coal fly ash and palm oil fuel ash into the mixture as "filler" materials. Both coal fly ash and palm oil fuel ash are also abundant industrial wastes found in Mindanao, Philippines (Tigue et al., 2018).

The development of Au mine tailings-based geopolymers is a sustainable way to recycle, repurpose and stabilize these wastes. In this study, ASGM tailings were stabilized by geopolymerization using coal fly ash, palm oil fuel ash and a powder-based alkali activator. Specifically, this study aims to: (1) identify toxic and hazardous elements found in ASGM tailings, (2) determine the physico-chemical, mineralogical and morphological characteristics of synthesized geopolymer and (3) elucidate the geochemical stability of hazardous and toxic elements from the tailings after geopolymerization. The first and second objectives were achieved by detailed characterization of tailings and tailings-based geopolymer samples by X-ray fluorescence spectroscopy (XRF), X-ray powder diffraction (XRD), attenuated total reflectance Fourier transform spectroscopy (ATR-FTIR), scanning electron microscopy with energy-dispersive X-ray spectroscopy (SEM-EDS), and standard compressive strength test while the third objective was accomplished by subjecting the tailings and tailings-based geopolymer to the toxicity characteristic leaching procedure (TCLP).

2. Materials and methods

2.1. Sampling and preparation of starting materials

The ASGM tailings (MT) sample was collected in an open '*dampacan*' or impoundment of ASGM plant located in Rosario, Agusan del Sur, Philippines while the sugar-mill lime sludge (LS) and coal fly ash (FA) were obtained from a sugar manufacturing company and a coal-fired power plant located in the provinces of Bukidnon and Misamis Oriental, Philippines, respectively. Meanwhile, palm oil fuel ash (PF) was also collected from a palm milling company in Bukidnon, Philippines. The ASGM plant employed combination of amalgamation and cyanidation in the recovery process of gold as show in the illustration in Figure 1 (a). The sampling site and raw materials used were shown in Figure 1 (b). Collection and preservation of samples were done following ASTM-D4220 (Standard practices for preserving and transporting soil samples). Sampling was done using an auger drill at random points on the impoundment area. Collected samples were placed in a plastic bag with zip-lock cover as tightly as possible by squeezing out the air. After sealing, the bags were then put in a container protected from direct exposure to heat. All starting materials were air-dried and sieved through a 2-mm aperture screen prior to characterization and geopolymerization. Analytical grade NaOH pellets and glacial acetic acid were also used in this study.

2.2. Preparation of the powder-based alkali activator

The preparation of powder-based alkali activator (PA) was based on the procedure used in our previous study (Aseniero et al., 2019). The dry activator was synthesized by mixing LS with 5 M NaOH at a 0.5 ratio by weight for 10 min using a rotary mixer until a homogenous mixture was obtained. The paste was then oven-dried for 8 h at 80 °C to accelerate the formation of reaction products. After drying, it was cooled, pulverized and sieved to obtain the less than 150 μm size fraction. NaOH was selected as an activating solution because it is widely available and is known as a good solvent of silicate and aluminate monomers (Khale and Chaudhary, 2007; Singhi et al., 2016).

2.3. Synthesis of geopolymer product

Geopolymer mixtures were prepared using the mixing ratio shown in Table 1, which were then mixed with 20% of water equivalent to the total weight of the dry mixture and stirred in a rotary mixer for at least 10 min. The amount of FA and PF added was fixed at 10 % of the total mass as it

Table 1. Geopolymer mixing design.

Sample ID	MT (%)	FA (%)	PF (%)	PA (%)
GP-FA	40	10	0	50
GP-PF	40	0	10	50

MT-mine tailings, FA-Fly Ash, PF-palm oil fuel ash, PA-powder activator.

shows to have the acceptable consistency of semi-paste character. Higher amount of these filler materials requires higher water content which lessen the strength of the resulting geopolymer. The resulting geopolymer pastes were poured into a non-reactive 50-mm cubic mold and placed on a vibrating table for 2 min to remove entrapped air. The molds were then covered to avoid direct loss of water and stored under ambient conditions. After 5 days setting, the geopolymers were de-molded, allowed to cure for 14 days under ambient temperature and then analyzed for their unconfined compressive strength as well as their physico-chemical, mineralogical and morphological properties.

2.4. Characterization of samples and geopolymer products

Particle sizes of all starting materials were determined using laser diffraction (Microtrac® MT3300SX, Nikkiso Co., Ltd., Japan) while the chemical compositions of the starting materials and synthesized geopolymers were determined by X-ray fluorescence (<50 μm loose powder) (NEXCG, Rikagu Corporation, Japan). For the ATR-FTIR spectroscopy analysis, the samples were ground manually to <10 μm using an agate mortar and pestle and then analyzed by an FT/IR-6200 HFV and ATR Pro One® attachment equipped with a diamond prism (Jasco Analytical Instruments, Japan) in the range of 400–4000 cm^{-1}. The mineralogical compositions of the samples were identified using XRD (MultiFlex, Rigaku Corporation, Japan) on pressed powders. The samples were also analyzed by SEM-EDS (InTouchScope™, JSM-IT200, JEOL Ltd., Japan) to identify minerals and phases incorporating the toxic and hazardous elements.

2.5. Mechanical performance of synthesized geopolymers

Synthesized geopolymer were tested for their unconfined compressive strength after 14 days of curing using a compression machine. Before testing, the cross-sectional areas of the samples were measured and after testing, the crushed samples were collected for characterization and the leaching experiments.

2.6. Leaching procedure

The toxicity characteristics leaching procedure (TCLP) was employed to determine the leachability of selected toxic trace elements from the AGSM tailings and synthesized geopolymer (USEPA 1311). Representative samples were mixed with a 0.57% acetic acid solution at a liquid-to-solid ratio of 20 and the suspensions were shaken for 12 h at 50 rpm under ambient conditions. The leachates were collected by vacuum filtration using 0.45 μm MCE membrane filters. Determination of the concentrations of selected elements was conducted using an inductively coupled plasma optical emission spectroscopy (ICP-OES, Agilent 5100, Argilent Technologies, Inc., USA) (margin of error = ±2%).

3. Results and discussion

3.1. Characterization of starting materials

3.1.1. Particle size analysis

All starting materials are less than 150 μm as seen in Figure 2. Among the three samples, PA (D_{80} = ~13 μm) had the finest size distribution while MT was the coarsest at D_{80} of ~33 μm. D_{80} is a parameter expressing that 80% of the mass of material is below a certain size. One important factor to consider in choosing a good source material for geopolymerization is its grain size. Assi et al. (2018) reported better mechanical strengths of geopolymers with finer particle because fewer air pockets and micro-cracks are created resulting in a denser microstructure. Furthermore, the MT sample predominantly contained clay-sized particles with minor amounts of silty-sand particles.

3.1.2. Physico-chemical, mineralogical and morphological characteristics of starting materials and identification of minerals containing toxic elements and heavy metals in ASGM tailings

The main component of MT is silicon (Si) (as SiO_2) which constitutes almost 40% of the total composition and aluminum (Al) (as Al_2O_3) makes up 10% as shown in Table 2. These two elements are important because they are the primary ingredients of a good geopolymer matrix. The Si/Al is close to the ideal ratio suggested by Davidovits et al. (2013), which further confirms the huge potential of ASGM tailings for geopolymer applications. Meanwhile, the presence of calcium (Ca) (as CaO) in the starting materials is advantageous because of its role in the formation of hydration products such as calcium silicate hydrate (CSH) and calcium aluminate silicate hydrate (CASH), both are well-known for the mechanical strength they impart on concrete materials. Excessive amounts of Ca, however, may accelerate the hardening of GP and cause incomplete geopolymerization (Zhao et al., 2019). To minimize the unwanted reduction in mechanical properties due to Ca, FA and PF were added as filler materials to adjust the Si-to-Al ratio around the optimum values. Moreover, XRF detected 34.61 mg/kg Hg in the ASGM tailings, which could be attributed to residual Hg used during amalgamation to recover gold (Opiso et al., 2018). Aside from Hg, toxic metalloids like As and hazardous heavy metals such as Zn, Pb, Cu and Cd were also detected in MT. The elevated amounts of these five environmentally regulated elements could be attributed to sulfide minerals (e.g., pyrite and chalcopyrite) present in the Au ore, which are well-known for their high heavy metal contents especially when formed under hydrothermal conditions (Duc et al., 2021; Park et al., 2019; Tabelin et al., 2014a, b).

Vibrational bands associated with Al and Si in the mid to low IR range (between 1500 and 450 cm^{-1}) imply the abundance of Al- and Si-bearing minerals (Figure 3). Characteristic IR bands associated with Al-silicates

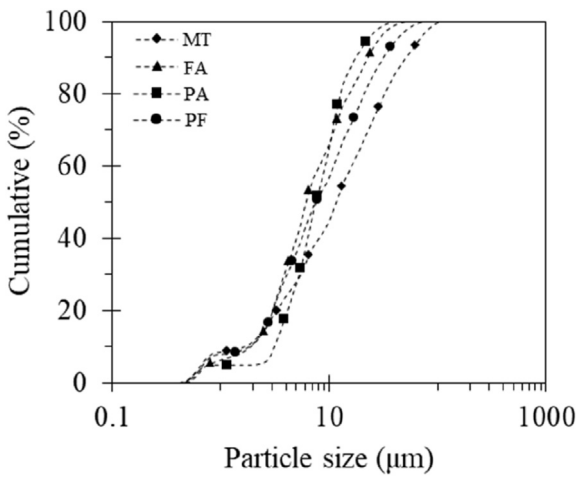

Figure 2. Particle size distribution of starting materials.

Table 2. Chemical compositions of starting materials.

Chemical Compound (wt%)	MT	PA	FA	PF
SiO_2	39.8	5.06	47.6	46.2
Fe_2O_3	21.2	0.242	12.2	5.47
Al_2O_3	9.81	1.43	22.1	10.4
SO_3	16.8	3.48	3.43	0.67
CaO	6.71	44.4	10.8	7.4
Na_2O	-	12.4	-	7.28
Hg (mg/kg)	34.61	-	-	0.076
Zn (mg/kg)	1990	1320	3120	1265
Cd (mg/kg)	20.8	-	-	-
Pb (mg/kg)	87.1	0.0165	0.632	0.052
Cu (mg/kg)	120	14.21	-	64
As (μg/kg)	0.0314	-	0.0023	0.0001
Si/Al	4.1	3.5	2.2	4.4

include the broad peak between 1150 and 950 cm^{-1}, which is assigned to the asymmetric stretching vibration of Si–O–Al or Al–O–Si and the absorption band at 776 cm^{-1} is attributed to the tetrahedral-tetrahedral ion vibration of silicates (Tabelin et al., 2017b; Xu et al., 2014). Moreover, Si–O asymmetrical bending vibration was detected at 693 cm^{-1} while the high intensity of the Si–O asymmetrical bending vibration detected in the diagnostic region, 820–740 cm^{-1}, is attributed to the presence of quartz (Saikia et al., 2008). The absorption bands observed at the region of 874 cm^{-1} and 693 cm^{-1} correspond to various vibrational bands associated with Al-oxyhydroxides/oxides (Park et al., 2018b; Tabelin et al., 2017c). The presence of Al-silicate minerals is also inferred by IR absorption bands in the high infrared region. The peak at 3620 and 2510 cm^{-1}, for

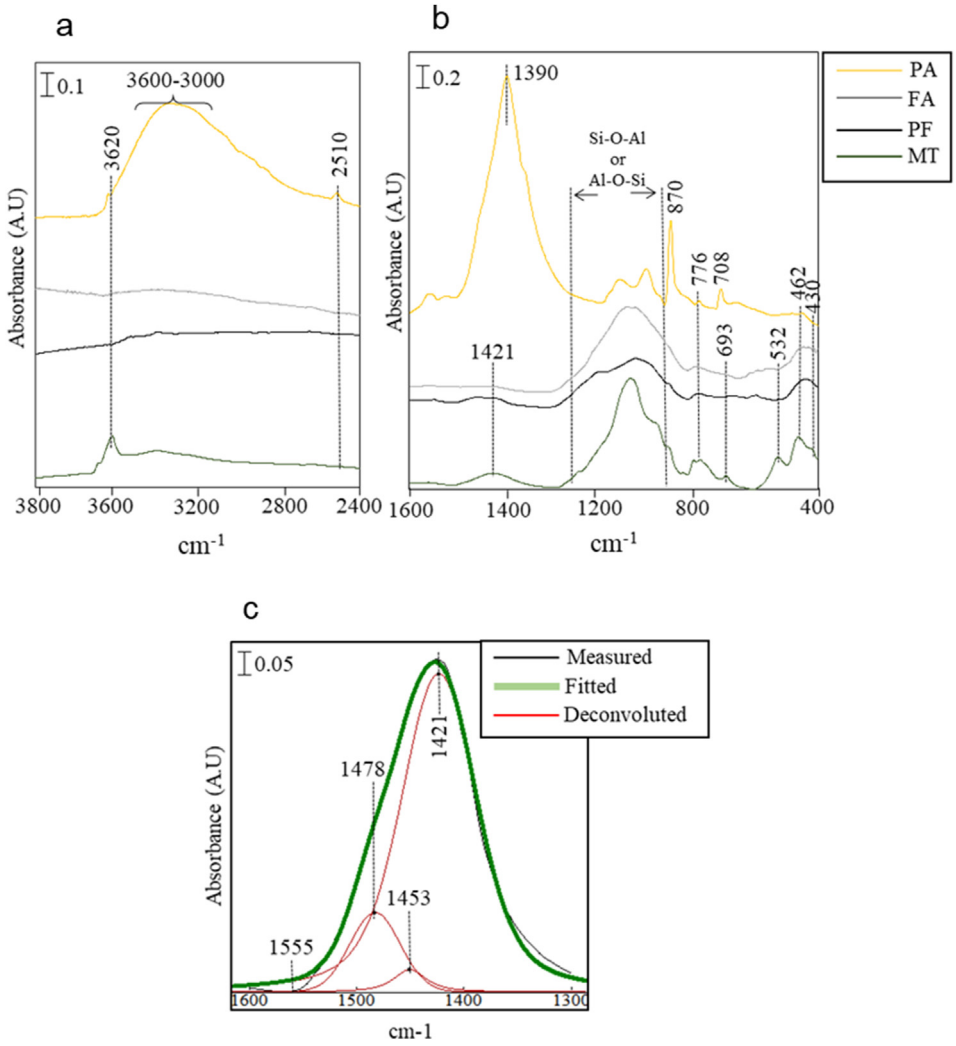

Figure 3. FTIR spectra of starting materials (a) 4000–2400 cm-1, (b) 1600 - 400 cm-1, (c) 1600–1300 cm-1, deconvoluted spectra between 1600 and 1200 of mine tailing.

example, could be attributed to Al–O–H stretching and Si–O–Si stretching, respectively (Park et al., 2018b; Tabelin et al., 2017d).

As for the broad peak between 3000 and 3700 cm^{-1}, this is assigned to O–H vibrations of crystalline and/or free water molecules (Tabelin et al., 2017c; Zoleta et al., 2020). The presence of carbonate minerals is also implied by the broad IR absorption peak between 1600 and 1300 cm^{-1} in PA and MT. Deconvolution of this peak in the MT sample using Gaussian fitting (Wojdyr, 2010) revealed C–O absorption bands of calcite (1421 cm^{-1}) and aragonite (1453 cm^{-1}) (Tabelin et al., 2017d). Similarly, PA exhibited a strong peak in this IR region, which could be attributed to its high carbonate content. The MT sample also exhibited a clear peak at 430 cm^{-1} assigned to S–S vibration in pyrite (Tabelin et al.,

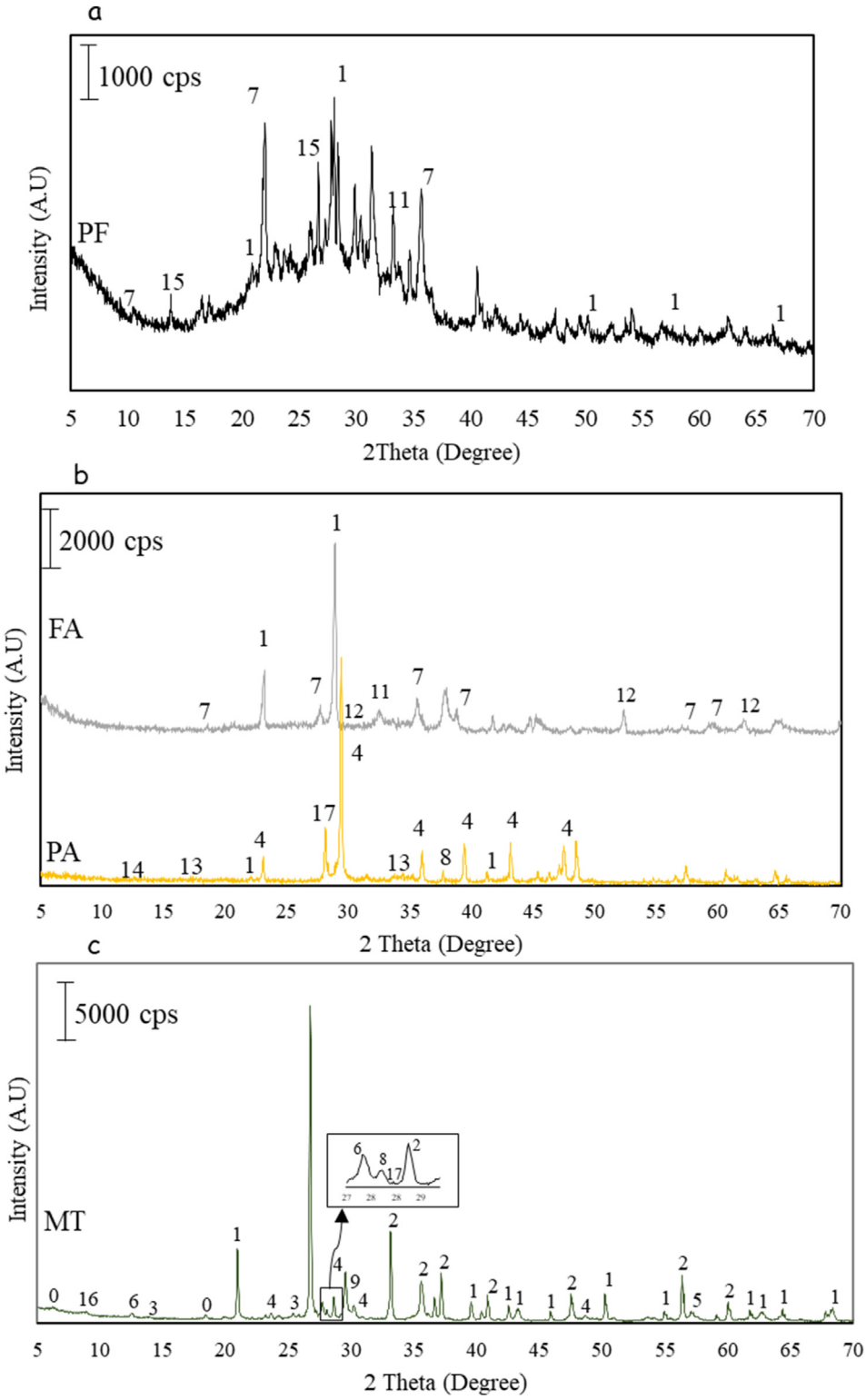

Figure 4. XRD patterns of (a) Palm oil fuel ash, (b) Fly ash and Powder activator, and (c) Mine Tailings. (Note: 1:quartz, 2:pyrite, 3:kaolinite, 4:calcite, 5:magnetite, 6:zeolite, 7:muscovite, 8:Lime, 9:chalcopyrite, 0:vermiculite, 11:dolomite, 12:maghemite, 13:portlandite and 14:sodium nitrate, 15:mullite, 16: montmorillonite and 17:anorthite).

2017c). Meanwhile, the absorption bands at 955, 532 and 462 cm^{-1} are assigned to Fe–O stretching of the Fe-oxyhydroxides/oxides (Tabelin et al., 2019; Yuniati et al., 2015), the presence of which could be explained by the oxidation of pyrite once exposed to the air (Park et al., 2019; Tabelin et al., 2018).

Based on the XRD results of the MT sample (Figure 4c), it contains quartz (SiO_2), pyrite (FeS_2), calcite ($CaCO_3$), magnetite (Fe_3O_4), kaolinite ($Al_2Si_2O_5(OH)_4$), zeolite, muscovite ($KAl_2(FOH)_2$ or $(KF)_2(Al_2O_3)_3(SiO_2)_6$), vermiculite, anorthite ($CaAl_2Si_2O_8$) and chalcopyrite ($CuFeS_2$) are present. Semi-quantitative analysis of this waste using Match!® (Crystal Impact, Germany) revealed that it is mainly composed of quartz at about 51%. Quartz is nonreactive in geopolymerization and only acts as internal fillers. The presence of calcite and lime in MT could be attributed to the use of hydrated lime to control the pH during Au extraction via cyanidation (Aseniero et al., 2019) while in PA are due to the initial content of sugar mill lime sludge (Opiso et al., 2017). Hydrated lime can easily be transformed into calcite in water. Furthermore, aluminum phyllosilicates or clay minerals have been established to be reactive during alkali activation since it readily dissolves in concentrated alkali solutions (Nikolov et al., 2017). Additionally, these minerals are responsible for the cross-linking between the polymeric chains to form a 3-D geopolymer network (Melo et al., 2017). However, the MT sample had relatively low quantity of these minerals (kaolinite = 1.9 %, zeolite = 1.3 %, muscovite = 0.9% and vermiculite = 0.2%). This could explain why geopolymer produced by Aseneiro et al. (2019) directly from Au mine tailings had relatively low compressive strengths (<5MPa). Figure 4 also presents the XRD patterns of FA and PF, which illustrate that these industrial wastes contain relatively abundant aluminium-silicate minerals like muscovite and mullite and their addition into the mixture could improve the final mechanical strength of geopolymer.

The MT sample also contains iron-bearing minerals such as pyrite, magnetite and chalcopyrite, which are consistent with the Fe–O, O–H and S–S absorption bands detected by ATR-FTIR. The elemental maps of MT particles also show several areas with strong signals of Fe and S in the same area (Figure 5), which are likely pyrite particles consistent with the detection of this mineral by XRD and ATR-FTIR. Point analyses of

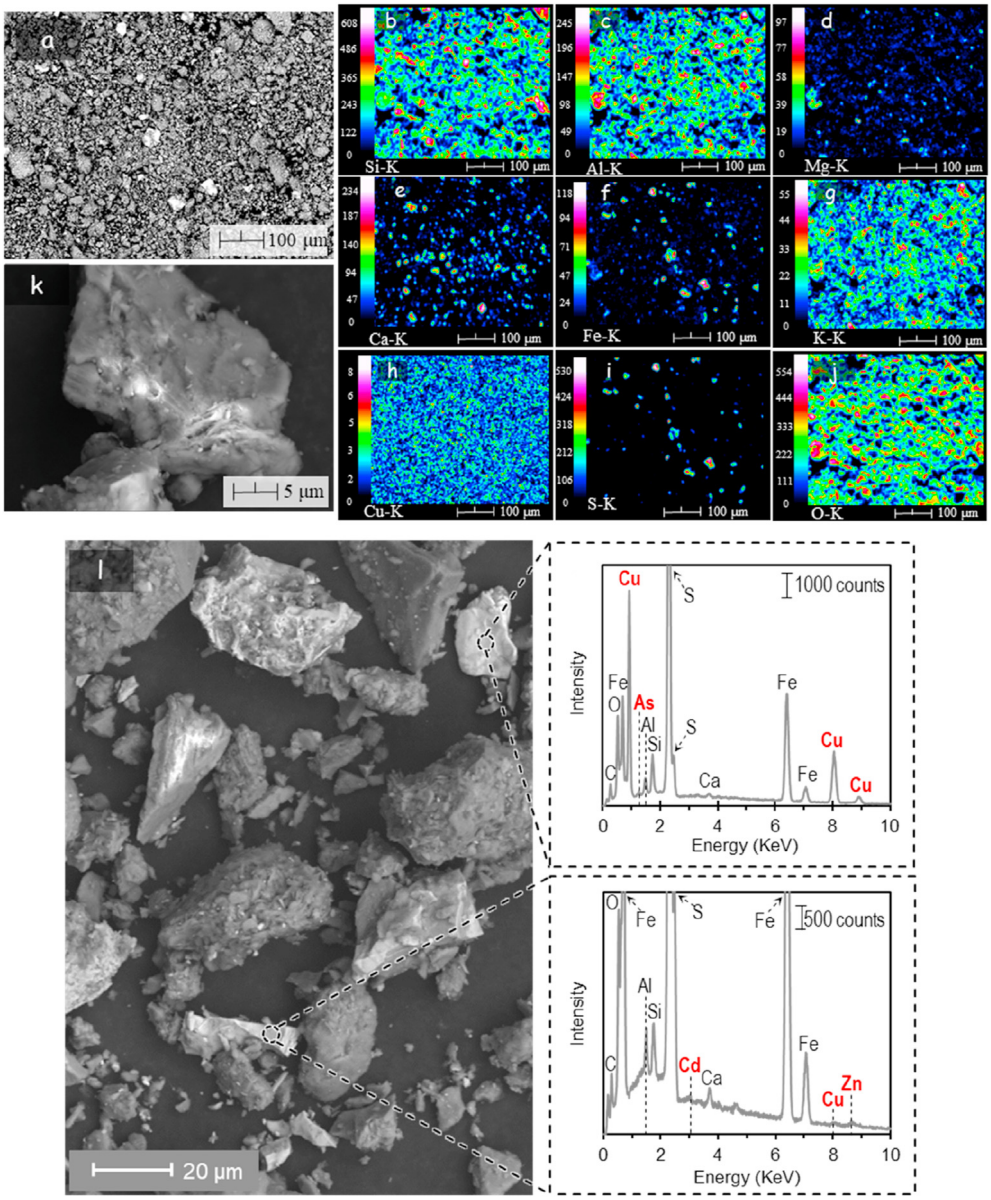

Figure 5. SEM photomicrograph of MT (a) and the corresponding elemental maps of Si (b), Al (c), Mg (d), Ca (e), Fe (f), K (g), Cu (h), S (i) and O (j); and photomicrograph of an aluminosilicate mineral showing plate-like structures (k) and Fe–S particles in the MT sample and the corresponding point analysis of representative Fe–S particles. (l).

representative Fe–S particles suggest that the sulfide minerals like pyrite and chalcopyrite contain not only Fe and Cu but also toxic elements like As and Cd as well as other heavy metals like Zn. These results suggest that most of the toxic and hazardous elements detected by XRF are likely hosted by sulfide minerals in the MT sample. Even in minor to trace amounts, sulfide minerals play crucial roles in the mobility of environmentally regulated elements like As, Cd, Cu and Zn as noted by several authors (Kamata and Katoh, 2019; Mar et al., 2013; Silwamba et al., 2020a, b; Tabelin et al., 2010, 2012d; 2014b; 2017b). Kamata and Katoh (2019), for example, reported that the release of As and heavy metals like Cu, Zn and Pb from marine sedimentary rocks is strongly influenced by the oxidation of sulfide minerals and the subsequent precipitation of iron-oxyhydroxides. Similarly, Huyen and coworkers (2019a) noted the crucial role played by pyrite as either a sink or source in organic-rich sediment layers of the Mekong Delta depending on geochemical conditions. Furthermore, the MT sample is characterized by fine particles that are agglomerated together and/or attached to the surface of coarser particles. Moreover, some particles exhibited plate-like structures that are typically observed in phyllosilicates (Huyen et al., 2019b). Meanwhile, FA is composed of spherical glass-like particles rich in Al, Si, Ca and O (Figure 6) while the PF sample had granular-shaped particles that are composed mainly of Ca, Al, Fe and Si (Figure 7). The particle size distribution of PA is more uniform than those of FA and PF and is predominantly composed of Ca, Al and Si (Figure 8), which is to be expected because of very strong XRD peaks of calcite in PA.

3.2. Characterization of geopolymer products

3.2.1. Physico-chemical, mineralogical and morphological characteristics of geopolymer

Chemical composition of synthesized geopolymer were examined using XRF (Table 3). Ca as CaO is the main component of the two types of geopolymer brick samples, which could be attributed to the high Ca content of the powder activator (PA). Between the two samples, GP-PF had twice as much Fe as that of GP-FA despite its high initial content in fly ash. These imply that the majority of Fe was not diluted in GP-PF after polymerization and were only adsorbed in the surface.

ATR-FTIR spectra of the geopolymer samples are shown in Figure 9 while the IR absorption band assignments are summarized in Table 4. The weak absorption band at 3620 cm^{-1} observed in both geopolymer samples is attributed to Al–O in Al-oxyhydroxides/oxides, which was also noted in MT (Figure 1). Meanwhile, the absorption peak around 3385–3380 and 3045–3040 cm^{-1} for GP-PF and GP-FA in the deconvoluted region were due to the O–H stretching vibrations consistent with the stretching vibration at 1640 cm^{-1} of adsorbed water. Moreover, the ATR-FTIR spectra showed a broad peak at 1005 cm^{-1} and sharp peaks at 702 and 710 cm^{-1} assigned to the asymmetric stretching vibration of Si–O–Al or Al–O–Si, which are characteristic IR absorption bands indicative of successful geopolymerization (Xu et al., 2014). Additionally, the peak attributed to the tetrahedral-tetrahedral ion vibration of silicates has been shifted from 776 to 796 cm^{-1} in both sample after geopolymerization, indicating the breaking down of chemical bonds during activation, reassembly through polymerization, and the formation of new amorphous products that constitute the geopolymer matrix (Xu et al., 2014). Deconvoluted region from 1200–800 cm^{-1} further illustrates the formation of these geopolymer reaction products. The peaks detected at 1104 and 952 cm^{-1} in GP-FA, as well as that at 1078 cm–1 in GP-PF, are all related to the asymmetric stretching of Si–O bonds (Rees, 2007). In addition, the broad peak observed at ~995 cm^{-1} in both samples could be attributed to the vibration of silicate species bonded with the powder activator (Rees, 2007). Meanwhile, some absorption bands retained even after geopolymerization such as the Si–OH bending or tetrahedral bending vibrations at 870 and ~853 cm^{-1} as well as those associated with Fe–O stretching (532 cm^{-1}), suggesting that some minerals are unaffected by the polymerization process and only acts as fillers. Finally, strong absorbance peak intensities were observed at 1401 cm^{-1} in GP-PF and 1407 cm^{-1} in GP-FA, which correspond to C–O vibrations in carbonate minerals from PA.

As shown in Figure 10, it can be observed that there is a slight difference between the mineralogy of the two synthesized geopolymer. Although they are both predominantly composed of calcite (GP-PF = 44%, GP-FA = 44%), phyllosilicates are more prevalent in GP-PF. This could be attributed to the dominance of this type of minerals in PF compared to FA. Furthermore, vermiculite in MT, dolomite in FA and mullite in PF were absent in the mineralogy after geopolymerization. Vermiculite is known to transform to a phyllosilicate mica structure type in basic condition (Medri et al., 2015) while dolomite is known to dissolve during alkali activation regardless of the concentration of the

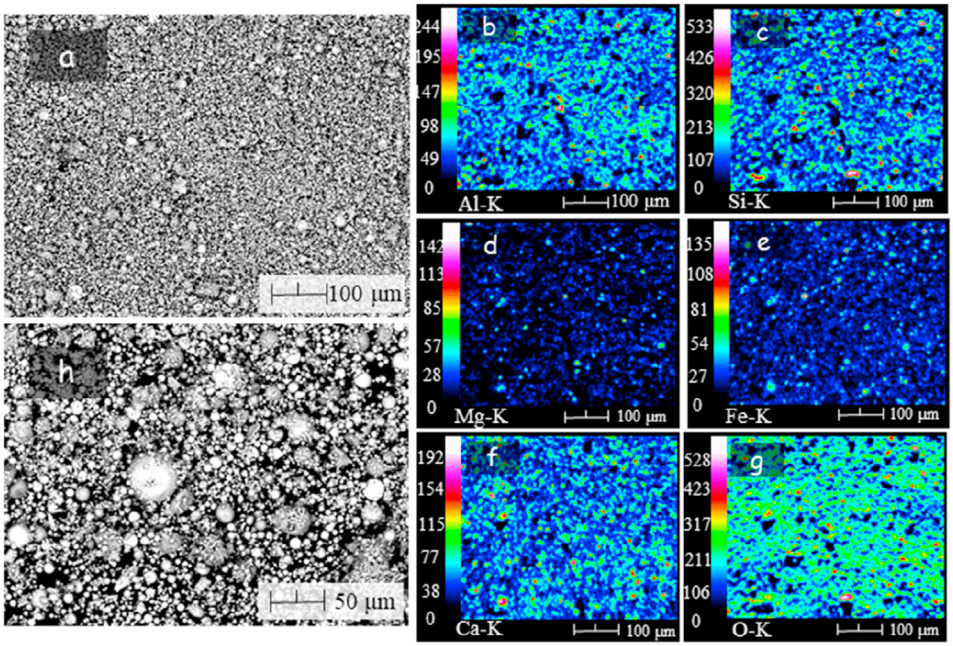

Figure 6. (a) SEM photomicrograph of FA and the corresponding elemental maps of Al (b), Si (c), Mg (d), Fe (e), Ca (f) and O (g). SEM photomicrograph of FA at higher magnification (h).

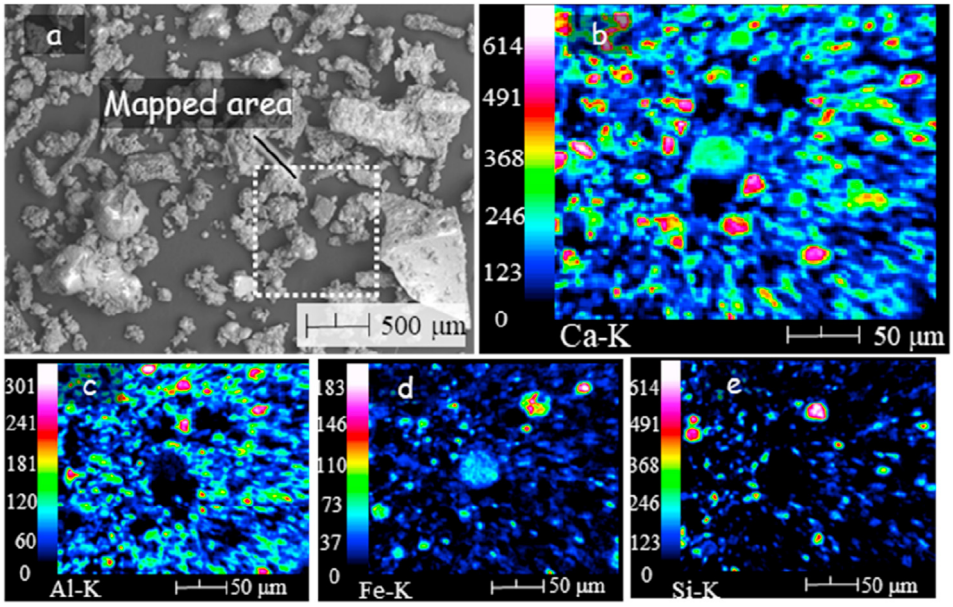

Figure 7. (a) SEM photomicrograph of PF and the corresponding elemental maps of Ca (b), Al (c), Fe (d) and Si (e).

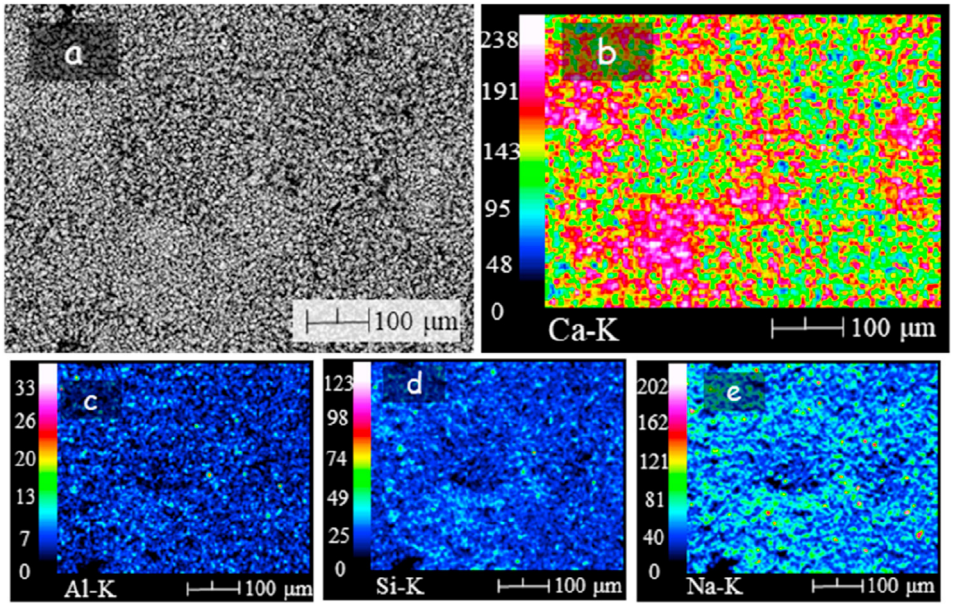

Figure 8. SEM photomicrograph of PA (a) and the corresponding elemental maps of Ca (b), Al (c), Si (d) and Na (e).

Table 3. Chemical composition of synthesized geopolymer bricks.

Chemical compound (wt%)	GP-FA	GP-PF
SiO_2	11.75	14.36
Fe_2O_3	15.89	35.25
Al_2O_3	8.54	4.84
SO_3	1.60	0.99
CaO	54.21	27.93
Na_2O	4.58	7.95
As (μg/kg)	0.01	-
Zn (mg/kg)	2421	3658
Pb (mg/kg)	85	163
PO_4	-	0.84

activators (Azimi et al., 2016). This indicates their participation during polymerization and polycondensation.

XRD results showed the absence of new clay mineral formation while some co-existing minerals were retained after geopolymerization such as magnetite (Fe_3O_4) in MT (Figure 4). This further implies that some crystalline minerals do not participate in the polymerization process and act only as internal fillers within the gel phase. Additionally, despite the high content of calcite and quartz in the starting materials, these minerals are known to be insoluble under basic conditions and completely remains in the geopolymer framework. Although these minerals do not chemically participate during geopolymerization, they could contribute to the mechanical performance of the geopolymer due to their very fine size (Ahmari and Zhang, 2012). Similar results were also obtained by Ren et al. (2015) for mine tailings-based geopolymer incorporated with

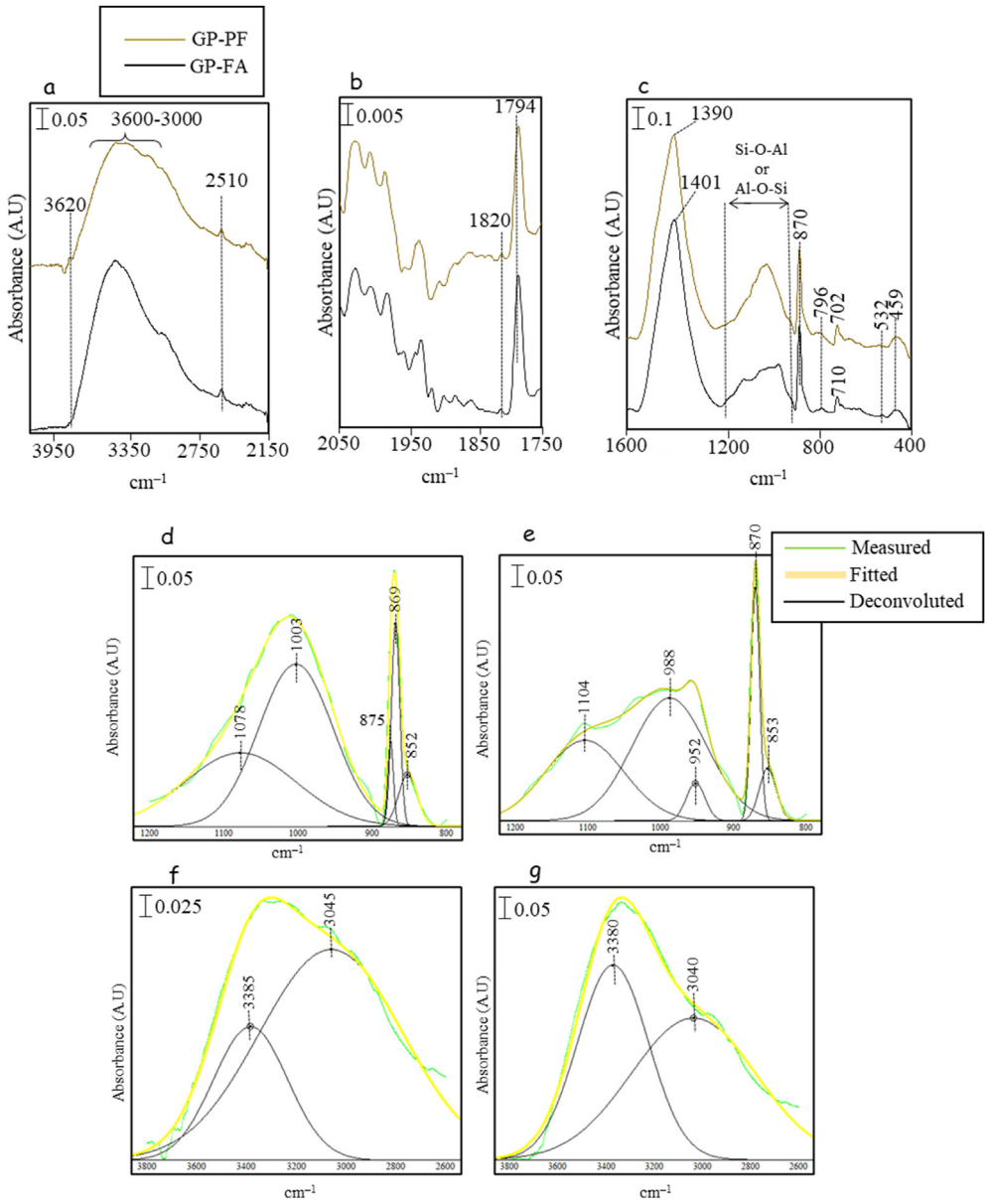

Figure 9. FTIR spectra of geopolymer bricks: (a) 4000–2150 cm^{-1}, (b) 2050–1750 cm^{-1}, (c) 1600–399 cm^{-1}, deconvoluted spectra in the 1200–800 and 3800–2600 IR range for GP-PF (d, f) and GP-FA (e, g).

aluminum sludge. The presence of the $Ca(OH)_2$ in MT induced the formation of calcium aluminum silicate hydrate (CASH) as detected in GP-PF, which is a big contributor in the improvement of physical properties of geopolymer. Formation of CASH could be due to the reaction of lime and clay minerals during reorganization and diffusion of dissolved ions in geopolymerization. Geopolymerization of MT also resulted in the reduction of peaks associated with pyrite and total absence of chalcopyrite via "dilution".

The synthesized geopolymers were also examined for their chemical and morphological characteristics using SEM-EDS as shown in Figure 11. Gel-like structures were observed, which are in agreement with those reported by Kiventera et al. (2016). These gel-like the amorphous to poorly crystalline are typically formed during geopolymerization. Furthermore, GP-FA appeared to be porous and some fly ash particles did not participate during geopolymerization. This is due to the presence of iron ferrites in FA that are very stable in basic condition. In general, the synthesized geopolymers showed mostly a homogenous microstructure characteristic indicating that the mine tailings particles were embedded in the geopolymer matrix.

Ca, Na and O dominated the whole mapped area indicating their high abundance consistent with the XRF and XRD results. Ca, Si and Al existed in the same area demonstrating a calcium aluminum silicate hydrate (CASH) product. Meanwhile, Al, Si, K, Mg and O can also be observed in the same regions, which could be due to the presence of clay minerals. Strong signals of Fe and S at the same region were also observed in the morphology of both geopolymer samples. Similar signals were detected in MT (Figure 4), which is attributed to the presence of iron-sulfide minerals such as pyrite or chalcopyrite. The SEM-EDS results imply that sulfide minerals were encapsulated or trapped in the framework of the geopolymer.

3.2.2. *Unconfined compressive strength of geopolymers*

The unconfined compressive strength (UCS) of the synthesized geopolymer at 14 days curing were investigated in this study

Table 4. Potential peak assignment of IR bond vibration for GP.

Theoretical Wavenumber (cm^{-1})	Actual wavenumber (cm-1)	Assignment	Reference
3620	3620	Al–OH stretching vibration	Koshy et al. (2018), Tabelin et al. (2017c)
3000–3600	3360	O–H stretching vibration of hydroxyl group	Moukannaa et al. (2018), Ren et al. (2015), Capasso et al. (2019), Ozen and Derum (2019), Tabelin et al. (2019)
1650–1600	1620	H–O–H bending vibration	Moukannaa et al. (2018), Ren et al. (2015)
1500–1400	1408	C–O stretching vibration in Na_2CO_3 and $CaCO_3$	Ma et al. (2019), Ozen and Derum (2019), Aboulayt et al. (2017), Ren et al. (2015), Moukannaa et al. (2018), Tabelin et al. (2017b)
1100–800	1010	Si–O–Si, Si–O–Al or Al–O–Si stretching vibrations	Capasso et al. (2019), Ma et al. (2019) Koshy et al. (2018), Moukannaa et al. (2018)
881–870	870	Si–OH bending mode or tetrahedral bending Al	Koshy et al. (2018)
800–770	796	Si–O–Si symmetric stretching	Moukannaa et al. (2018)
~780	779	Tetrahedral units of Al	Ozen and Derum (2019)
740–690	711	Si–O–Al or Al–O–Si symmetric stretching vibration	Koshy et al. (2018), Park et al. (2018b)
~532	532	Si–O–Si stretching vibration	Moukannaa et al. (2018)
470–450	459	Fe–O Stretching Vibration	Tabelin et al. (2019)

(Figure 12). The average UCS of GP-FA and GP-PF were 7.58 and 7.7 MPa, respectively. GP-PF had higher UCS because of the formation of CASH reaction products, which could improve strength formation similar to that reported in concrete (Zhao et al., 2019). Although the same procedure was employed, tests results in this study were much higher compared to our previous study (Aseniero et al., 2019). The increase could be attributed to the addition of quartz/silica and aluminosilicates found in PF and FA that readily participated during geopolymerization. According to He et al. (2016), increasing the Si–O–Si bonds and residual silica as reinforcement resulted in higher mechanical strength because of the less porous microstructure. Therefore, the strength of the synthesized geopolymer bricks suggests that it could be utilized for various construction applications such as production of paving blocks and wall partitions as well as possible raw materials for the production of geopolymer cement.

3.3. Leachability of selected toxic trace elements from the synthesized geopolymers

The TCLP results of selected elements from the starting materials and geopolymer samples are presented in Table 5. According to the regulatory standard requirements of TCLP set by the United States Environmental Protection Agency (USEPA) and Hazardous waste management section of the Department of Environmental and Natural Resources (DENR) of the Philippines, MT is not in compliance with respect to the leachability of As and Pb and could be classified as a hazardous material. Additionally, the minimal concentration of cyanide (CN^-) was detected in the leachate of MT after TCLP, indicating that Au-mine tailings from Rosario, Agusan del Sur still contains CN^- despite its constant exposure to direct sunlight.

Meanwhile, TCLP results for the geopolymer brick samples showed lower concentrations of toxic heavy metals. Additionally, concentrations

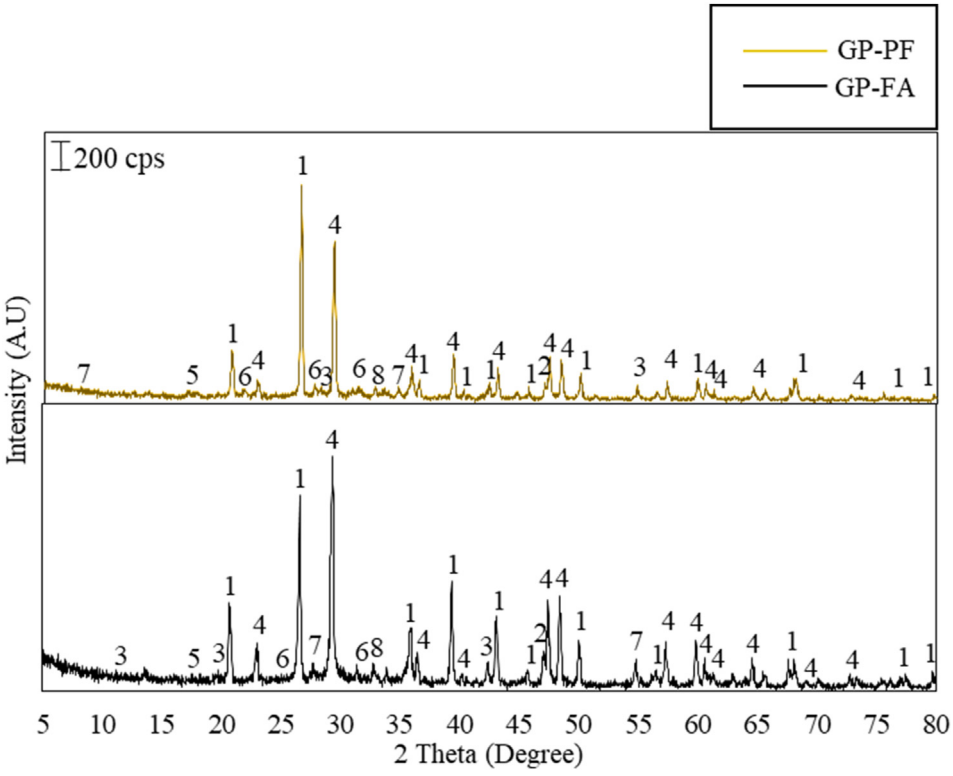

Figure 10. XRD patterns of synthesized geopolymers. Note, 1:quartz, 2:pyrite, 3:kaolinite, 4:calcite, 5:magnetite, 6:zeolite, 7:muscovite, and 8:calcium aluminum silicate hydrate.

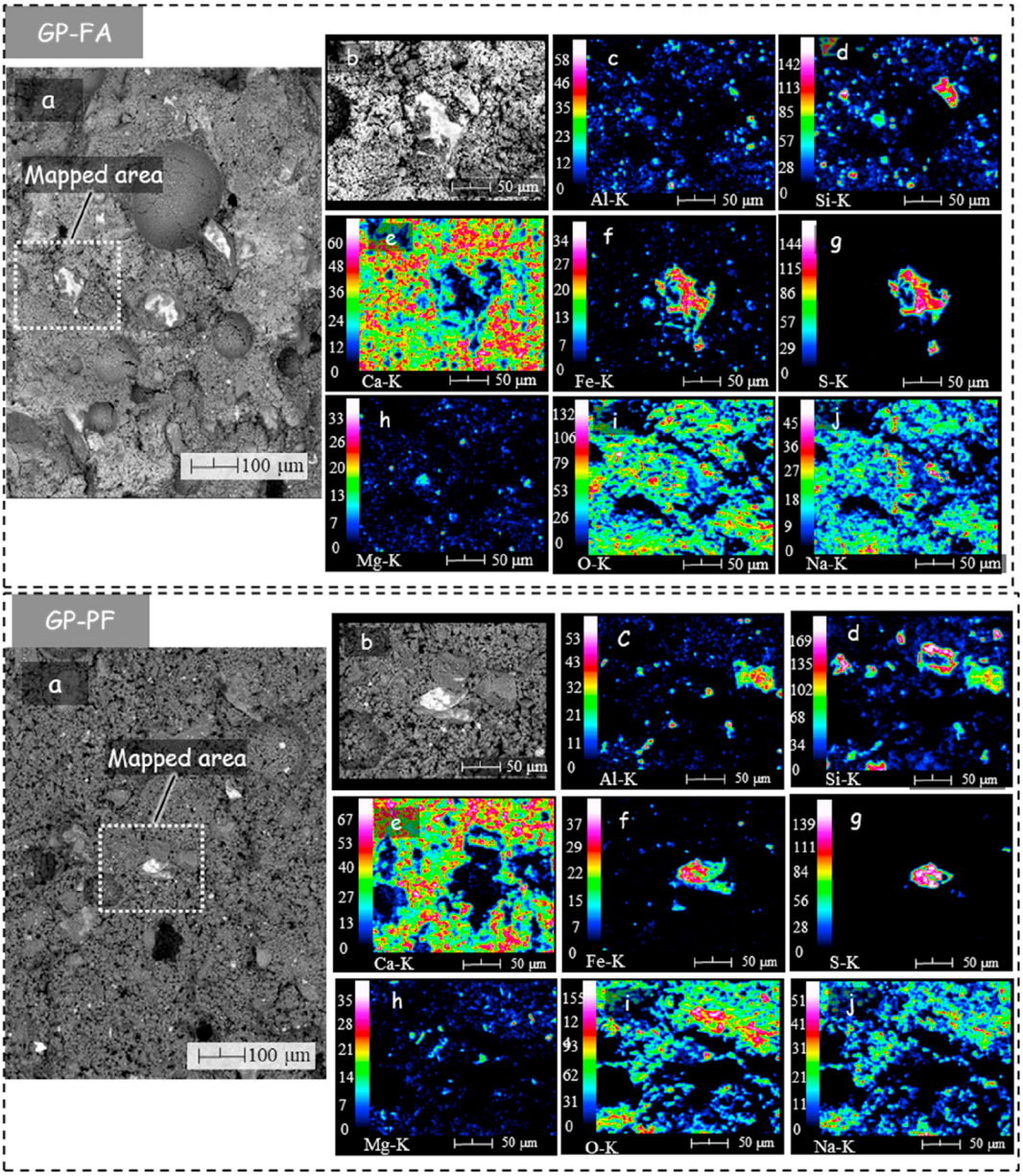

Figure 11. SEM photomicrograph of GP-FA and GP-PF (a) and mapped area (b) with corresponding elemental maps of Al (c), Si (d), Ca (e), Fe (f), S (g), Mg (h), O (i) and Na (j).

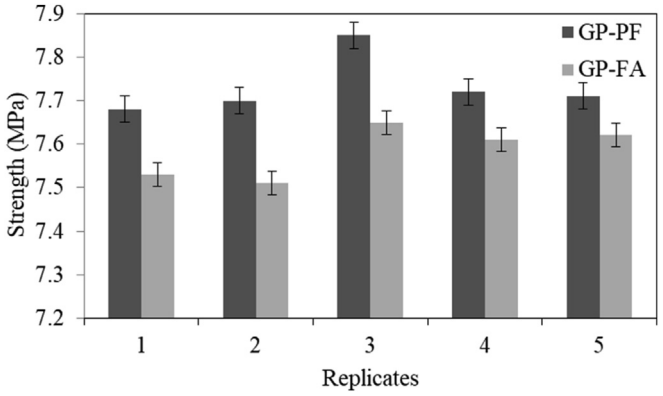

Figure 12. Unconfined compressive strength of geopolymer bricks.

were below the regulatory standards required by USEPA and DENR. These results suggest that the synthesized geopolymers can be safely used for construction applications. The very low leachabilities of As, Pb and Fe in both geopolymer materials suggest that the MT sample was effectively encapsulated within the geopolymer matrix. The incorporation of hazardous toxic elements such as As, Pb and Se were best achieved by GP-FA whereas Cd was effectively immobilized by GP-PF. It is interesting to note that the leaching of Cd was more extensive in GP-FA than GP-PF, which could be attributed to the addition of Cd-bearing FA.

4. Conclusion

The results of this study have several important implications as to the geopolymerization of mine tailings (MT) blended with fly ash (FA), palm oil fuel ash (PF) and sugar mill lime sludge (LS) as Ca-based dry powder activator. First, the physico-chemical properties of MT suggest its applicability as good source material for geopolymerization, but the addition of other waste material such as FA, PF and the use of Ca-based powder

Table 5. Concentrations of leached metals (mg/L).

Elements	DENR limit	USEPA limit	MT	FA	PA	PF	GP-FA	GP-PF
As	2.8	5	29.5	0.591	0.543	0.499	0.494	0.102
Hg	4	0.2	0.01	<0.01	<0.01	<0.01	<0.01	<0.01
Pb	4	5	373	0.715	0.351	0.545	0.402	0.459
Se	4	1	0.962	<0.01	<0.01	0.021	0.049	0.054
Cd	-	1	0.243	0.019	<0.01	<0.01	0.093	0.098
Cr	-	5	<0.01	<0.01	<0.01	<0.01	<0.01	<0.01
Cu	-	-	5.43	15.8	0.331	12.7	2.28	1.66
Fe	-	-	1340	497	409	804	16.0	93.7
Zn	-	-	12.8	17.3	4.07	15.4	17.6	0.931
Ca	-	-	27000	9220	78100	8560	4460	7580
Si	-	-	689	168	200	2230	198	342
Al	-	-	380	126	21	141	26.6	81
Na	-	-	60	13500	18680	15245	6729	7478
Mg	-	-	130	5442	519	6370	65.6	63.5
Mn	-	-	624	173	19.3	178	21.6	8.72
K	-	-	10	20865	1865	23455	1134	181
P	-	-	<0.01	7530	85	7005	57.5	12.6
CN-	-	-	1.16	ND	ND	ND	<0.1	<0.1

Note: "ND" means not determined, <0.01 is the detection limit of ICP-OES, and <0.1 is the detection limit of AAS. MT-mine tailings, FA-Fly Ash, PF-palm oil fuel ash, PA-powder activator, GP-FA – geopolmer with fly ash, GP-PF – geopolymer with palm oil fuel ash.

activator are necessary to enhance the matrix of the resulting geopolymer. Second, the reaction products associated with geopolymerization shows that some initial content of starting materials retained after alkali activation. This indicates that some minerals only act as internal fillers and do not participate during reorganization and polycondensation. Third, it was also evident that toxic heavy metals and iron sulfide minerals such as pyrite and chalcopyrite were embedded within the geopolymer matrix based from the microstructural and mineralogical analyses. This suggests that geopolymerization of MT is an effective stabilization or immobilization technique of toxic heavy metals. Fourth, the unconfined compressive strength test also shows that both geopolymer samples have promising unconfined compressive strength. This implies that geopolymerization of ASGM tailings could be repurposed for construction application such as paving blocks and wall partitions for low-cost housing applications.

Declarations

Author contribution statement

Einstine M. Opiso: Conceived and designed the experiments; Performed the experiments; Analyzed and interpreted the data; Contributed reagents, materials, analysis tools or data; Wrote the paper.

Carlito B. Tabelin: Analyzed and interpreted the data; Wrote the paper.

Christian V. Maestre: Performed the experiments; Analyzed and interpreted the data; Wrote the paper.

John Paul J. Aseniero: Analyzed and interpreted the data; Contributed reagents, materials, analysis tools or data.

Ilhwan Park: Performed the experiments; Analyzed and interpreted the data.

Mylah Villacorte-Tabelin: Performed the experiments; Wrote the paper.

Funding statement

This work was supported by Department of Science and Technology – Philippine Council for Industry, Energy and Emerging Technology Research and Development (DOST-PCIEERD).

Data availability statement

Data included in article/supplementary material/referenced in article.

Declaration of interests statement

The authors declare no conflict of interest.

Additional information

No additional information is available for this paper.

Acknowledgements

The authors are grateful to the Central Mindanao University administration for the assistance during the duration of the research. Special acknowledgments are also due to the Department of Civil Engineering and Department of Physics for the moral support in the conduct of the study.

References

Abdel-Gawwad, Abo-El-Enein, 2016. A novel method to produce dry geopolymer cement powder. HBRC J. 12 (1), 13–24.

Abdul Rahim, R.H., Rahmiati, T., Azizli, K.A., Man, Z., Nuruddin, M.F., Ismail, L., 2015. Comparison of using NaOH and KOH Activated Fly ash -based geopolymer on mechanical properties. Mater. Sci. Forum 803, 179–184.

Aboulayt, A., Riahi, M., Ouazzani Touhami, M., Hannache, H., Gomina, M., Moussa, R., 2017. Properties of metakaolin based geopolymer incorporating calcium carbonate. Adv. Powder Technol. 28 (9), 2393–2401.

Ahmari, S., Zhang, L., 2012. Production of eco-friendly bricks from copper mine tailings through geopolymerization. Construct. Build. Mater. 29, 323–331.

Ahmari, S., Zhang, L., 2013. Durability and leaching behavior of mine tailings-based geopolymer bricks. Construct. Build. Mater. 44, 743–750.

Akagi, H., Castillo, E.S., Cortes-Maramba, N., Francisco-Rivera, A.T., Timbang, T.D., 2000. Health assessment for mercury exposure among schoolchildren residing near a gold processing and refining plant in Apokon, Tagum, Davao del Norte, Philippines. Sci. Total Environ. 259 (1-3), 31–43.

Appleton, J.D., Williams, U.,T.M., Breward, N., Apostol, A., Miguel, J., Miranda, C., 1999. Mercury contamination associated with artisanal gold mining on the island of Mindanao, the Philippines. Sci. Total Environ. 228, 95–109.

Appleton, J.D., Weeks, J.M., Calvez, J.P.S., Beinhoff, C., 2006. Impacts of mercury contaminated mining waste on soil quality, crops, bivalves, and fish in the Naboc River area, Mindanao, Philippines. Sci. Total Environ. 354, 198–211.
Aseniero, J.P., Opiso, E.M., Banda, M.H.B., Tabelin, C.B., 2019. Potential Utilization of artisanal gold-mine tailings as geopolymeric source material: a preliminary investigation. SN Appl. Sci. 1, 35.
Assi, L., Anay, R., Leaphart, D., Soltangharaei, V., Ziehl, P., 2018. Understanding Early Geopolymerization Process of Fly Ash–Based Geopolymer Paste Using Pattern Recognition. J. Mater. Civil Eng. 30 (6), 04018092.
ASTM D4220/D4220M-14, 2014. Standard Practices for Preserving and Transporting Soil Samples. ASTM International, West Conshohocken, PA. www.astm.org.
Azimi, E.A., Abdullah, M.M.A.L., Ming, L., Yong, H., Kamarudin, H., Aziz, I., 2016. Review of dolomite as precursor of geopolymer materials. MATEC Web Conf. 78, 01090.
Bayuaji, R., Yasin, A.K., Susanto, T.E., Darmawan, M.S., 2017. September. A review in geopolymer binder with dry mixing method (geopolymer cement). AIP Conf. Proc. 1887, 020022.
Caballero, E., Sanchez, W., Rios, C., 2014. Synthesis of geopolymers from alkaline activation of gold mining wastes. Ingenieria y Competitividad 16, 317–330.
Calderon, A.R.M., Alorro, R.D., Tadesse, B., Yoo, K., Tabelin, C.B., 2019. Evaluation of maghemite-rich iron oxide composite prepared from magnetite as adsorbent for gold from chloride solution. JOM 71 (12), 4639–4646.
Calderon, A.R.M., Alorro, R.D., Tadesse, B., Yoo, K., Tabelin, C.B., 2020. Repurposing of nickeliferous pyrrhotite from mine tailings as magnetic adsorbent for the recovery of gold from chloride solution. Resour. Conserv. Recycl. 161, 104971.
Capasso, I., Lirer, S., Flora, A., Ferone, C., Cioffi, R., Caputo, D., Liguori, B., 2019. Reuse of mining waste as aggregates in fly ash-based geopolymers. J. Clean. Prod. 220, 65–73.
Davidovits, F., Davidovits, J., Davidovits, M., 2013. Geopolymer cement of the calcium ferro-aluminosilicate polymer type and production process. Patent WO2012056125A1.
Duc, H.G., Tabelin, C.B., Tangviroon, P., Tamamura, S., Igarashi, T., 2021. Effects of cement addition on arsenic leaching from soils excavated from projects employing shield-tunneling method. Geoderma 385, 114896.
Ghenciu, A.F., 2002. Review of fuel processing catalysts for hydrogen production in PEM fuel cell systems. Curr. Opin. Solid State Mater. Sci. 6, 389–399.
Ghosh, S., Sullivan, C.A.W., Zerkowski, M.P., Molinaro, A.M., Rimm, D.L., Camp, R.L., Chung, G.G., 2008. High levels of vascular endothelial growth factor and its receptors (VEGFR-1, VEGFR-2, neuropilin-1) are associated with worse outcome in breast cancer. Hum. Pathol. 39 (12), 1835–1843.
Gitari, M.W., Akinyemi, S.A., Thobakgale, R., et al., 2017. Physicochemical and mineralogical characterization of musina mine copper and new onion gold mine tailings: implications for fabrication of beneficial geopolymeric construction of materials. J. Afr. Earth Sci. 137, 218–228.
He, P., Wang, M., Fu, S., Jia, D., Yan, S., Yuan, J., Xu, J., et al., 2016. Effects of Si/Al ratio on the structure and properties of metakaolin based geopolymer. Ceramics Int. 42 (13), 14416–14422.
Huang, D., Kilic, M., 2019. Gold, platinum, and expected stock returns. J. Financ. Econ. 132 (3), 50–75.
Huyen, D.T., Tabelin, C.B., Thuan, H.M., Dang, D.H., Truong, P.T., Vongphuthone, B., Kobayashi, M., Igarashi, T., 2019a. The solid-phase partitioning of arsenic in unconsolidated sediments of the Mekong Delta, Vietnam and its modes of release under various conditions. Chemosphere 233, 512–523.
Huyen, D.T., Tabelin, C.B., Thuan, H.M., Danga, D.H., Truong, P.T., Vongphuthone, B., Kobayashi, M., 2019b. Geological and Geochemical Characterizations of Sediments in Six Borehole Cores from the Arsenic-Contaminated Aquifer of the Mekong Delta. Vietnam. Data in Brief, p. 104230.
Igarashi, T., Salgado, P.H., Uchiyama, H., Miyamae, H., Iyatomi, N., Hashimoto, K., Tabelin, C.B., 2020. The two-step neutralization ferrite-formation process for sustainable acid mine drainage treatment: removal of copper, zinc and arsenic, and the influence of coexisting ions on ferritization. Sci. Total Environ. 715, 136877.
Jeon, S., Ito, M., Tabelin, C.B., Pongsumrankul, R., Kitajima, N., Park, I., Hiroyoshi, N., 2018a. Gold recovery from shredder light fraction of E-waste recycling plant by flotation-ammonium thiosulfate leaching. Waste Manag. 77, 195–202.
Jeon, S., Tabelin, C.B., Takahashi, H., Park, I., Ito, M., Hiroyoshi, N., 2018b. Interference of coexisting copper and aluminum on the ammonium thiosulfate leaching of gold from printed circuit boards of waste mobile phones, 2018. Waste Manag. 81, 148–156.
Jeon, S., Ito, M., Tabelin, C.B., Pongsumrankul, R., Tanaka, S., Kitajima, N., Saito, A., Park, I., Hiroyoshi, N., 2019. A physical separation scheme to improve ammonium thiosulfate leaching of gold by separation of base metals in crushed mobile phones. Miner. Eng. 138, 168–177.
Jeon, S., Tabelin, C.B., Takahashi, H., Park, I., Ito, M., Hiroyoshi, N., 2020a. Enhanced cementation of gold via galvanic interactions using activated carbon and zero-valent aluminum: a novel approach to recover gold ions from ammonium thiosulfate medium. Hydrometallurgy 191, 105165.
Jeon, S., Tabelin, C.B., Park, I., Nagata, Y., Ito, M., Hiroyoshi, N., 2020b. Ammonium thiosulfate extraction of gold from printed circuit boards (PCBs) of end-of-life mobile phones and its recovery from pregnant leach solution by cementation. Hydrometallurgy 191, 105214.
Kamata, A., Katoh, M., 2019. Arsenic release from marine sedimentary rock after excavation from urbanized coastal areas: oxidation of framboidal pyrite and subsequent natural suppression of arsenic release. Sci. Total Environ. 670, 752–759.
Khale, D., Chaudhary, R., 2007. Mechanism of geopolymerization and factors influencing its development: a review. J. Mater. Sci. 42, 729–746.
Khater, H.M., 2012. Effect of calcium on geopolymerization of aluminosilicate wastes. J. Mater. Civ. Eng. 24 (1), 92–101.
Kiventera, J., Golek, L., Yliniemi, J., Ferreira, V., Deja, J., Illikainen, M., 2016. Utilization of sulphidic tailings from gold mine as a raw material in geopolymerization. Int. J. Miner. Process. 149 (10), 104–110.
Koshy, N., Dondrob, K., Hu, L., Wen, Q., Meegoda, J.N., 2018. Synthesis and characterization of geopolymers derived from coal gangue, fly ash and red mud. Construct. Build. Mater. 206, 287–296.
Li, C., Sun, H., Li, L., 2010. A review: The comparison between alkali-activated slag (Si+Ca) and metakaolin (Si+Al) cements. Cem. Concr. Res. 40 (9), 1341–1349.
Li, X., Gao, M., Hiroyoshi, N., Tabelin, C.B., Taketsugu, T., Ito, M., 2019a. Suppression of pyrite oxidation by ferric-catecholate complexes: an electrochemical study. Miner. Eng. 138, 226–237.
Li, X., Hiroyoshi, N., Tabelin, C.B., Naruwa, K., Harada, C., Ito, M., 2019b. Suppressive effects of ferric-catecholate complexes on pyrite oxidation. Chemosphere 214, 70–78.
Löfås, S., Johnsson, B., 1990. A novel hydrogel matrix on gold surfaces in surface plasmon resonance sensors for fast and efficient covalent immobilization of ligands. J. Chem. Soc., Chem. Commun. (21), 1526–1528.
Lucarelli, F., Marrazza, G., Turner, A.P., Mascini, M., 2004. Carbon and gold electrodes as electrochemical transducers for DNA hybridisation sensors. Biosens. Bioelectron. 19 (6), 515–530.
Luukkonen, T., Věžníková, K., Tolonen, E.-T., Runtti, H., Yliniemi, J., Hu, T., et al., 2017. Removal of ammonium from municipal wastewater with powdered and granulated metakaolin geopolymer. Environ. Technol. 39 (4), 414–423.
Ma, C., Zhao, B., Guo, S., Long, G., Xie, Y., 2019. Properties and characterization of green one-part geopolymer activated by composite activators. J. Clean. Prod. 220, 188–199.
Mar, K.K., Karnawati, D., Putra, D.P.E., Igarashi, T., Tabelin, C.B., 2013. Comparison of Arsenic adsorption on lignite, bentonite, shale, and iron sand from Indonesia. Procedia Earth Planet. Sci. 6, 242–250.
Marove, C.A., Tangviroon, P., Tabelin, C.B., Igarashi, T., 2020. Leaching of hazardous elements from Mozambican coal and coal ash. J. Afr. Earth Sci. 103861.
Medri, V., Papa, E., Mazzocchi, M., Laghi, L., Morganti, M., Francisconi, J., Landi, E., 2015. Production and characterization of lightweight vermiculite/geopolymer-based panels. Mater. Des. 85, 266–274.
Melo, L.G.A., Periera, R.A., Pires, E.F.C., Darwish, F.A.I., Silva, F.J., 2017. Physicochemical characterization of pulverized phyllite rock for geopolymer resin synthesis. Mater. Res. 20, 236–243.
Moukannaa, S., Loutou, M., Benzaazoua, M., Vitola, L., Alami, J., Hakkou, R., 2018. Recycling of phosphate mine tailings for the production of geopolymers. J. Clean. Prod. 185, 891–903.
Nikolov, A., Rostovsky, I., Nugteren, H., 2017. Geopolymer materials based on natural zeolite. Case Stud. Construct. Mater. 6, 198–205.
Ojuri, O.O., Adavi, A.A., Oluwatuyi, O.E., 2016. Geotechnical and environmental evaluation of lime-cement stabilized soil-mine tailing mixtures for highway construction. In: Transportation Geotechnics.
Opiso, E.M., Sato, T., Otake, T., 2017. Microstructural properties of hardened cement paste blended with coal fly ash, sugar mill lime sludge and rice hull ash. Adv. Concr. Construct. 5, 289–301.
Opiso, E.M., Aseneiro, J.P.J., Banda, M.H.T., Tabelin, C.B., 2018. Solid-phase partitioning of mercury in artisanal gold mine tailings from selected key areas in Mindanao, Philippines, and its implications for mercury detoxification. Waste Manag. Res. 36, 269–276.
Ozen, M.Y., Derum, E.M., 2019. A Comparative Study: effect of different nanoparticles on the properties of gold mine tailings containing cement mortars. Construct. Build. Mater. 202, 396–405.
Paciotti, G.F., Myer, L., Weinreich, D., Goia, D., Pavel, N., McLaughlin, R.E., Tamarkin, L., 2004. Colloidal gold: a novel nanoparticle vector for tumor directed drug delivery. Drug Deliv. 11 (3), 169–183.
Park, I., Tabelin, C.B., Magaribuchi, K., Seno, K., Ito, M., Hiroyoshi, N., 2018a. Suppression of the release of arsenic from arsenopyrite by carrier-microencapsulation using Ti-catechol complex. J. Hazard Mater. 344, 322–332.
Park, I., Tabelin, C.B., Seno, K., Jeon, S., Ito, M., Hiroyoshi, N., 2018b. Simultaneous suppression of acid mine drainage formation and arsenic release by Carrier-microencapsulation using aluminum-catecholate complexes. Chemosphere 205, 414–425.
Park, I., Tabelin, C.B., Jeon, S., Li, X., Seno, K., Ito, M., Hiroyoshi, N., 2019. A review of recent strategies for acid mine drainage prevention and mine tailings recycling. Chemosphere 219, 588–606.
Park, I., Higuchi, K., Tabelin, C.B., Jeon, S., Ito, M., Hiroyoshi, N., 2021. Suppression of arsenopyrite oxidation by microencapsulation using ferric-catecholate complexes and phosphate. Chemosphere 269, 129413.
Phengsaart, T., Ito, M., Hamaya, N., Tabelin, C.B., Hiroyoshi, N., 2018. Improvement of jig efficiency by shape separation, and a novel method to estimate the separation efficiency of metal wires in crushed electronic wastes using bending behavior and “entanglement factor”. Miner. Eng. 129, 54–62.
Rajamane, N., Nataraja, M.C., Dattatreya, J.K., Lakshmanan, N., Sabitha, D., 2009. Geopolymer Concrete- a new eco-friendly material of construction. Masterbuilder 11, 200–206.
Rees, C.A., Provis, J.L., Lukey, G.C., van Deventer, J.S.J., 2007. Attenuated total reflectance Fourier transform infrared analysis of fly ash geopolymer gel ageing. Langmuir 23, 8170–8179.
Ren, X., Zhang, L., Ramey, D., Waterman, B., Ormsby, S., 2015. Utilization of aluminum sludge (AS) to enhance mine tailings-based geopolymer. J. Mater. Sci. 50, 1370–1381.
Saikia, B.J., Parthasarathy, G., Sarmah, N.C., 2008. Fourier transform infrared spectroscopic estimation of crystallinity in SiO2 based rocks. Bull. Mater. Sci. 31, 775–779.

Seng, S., Tabelin, C.B., Kojima, M., Hiroyoshi, N., Ito, M., 2019a. Galvanic microencapsulation (GME) using zero-valent aluminum and zero-valent iron to suppress pyrite oxidation. Mater. Trans. 60, 277–286.
Seng, S., Tabelin, C.B., Makino, Y., Chea, M., Phengsaart, T., Park, I., Hiroyoshi, N., Ito, M., 2019b. Improvement of flotation and suppression of pyrite oxidation using phosphate-enhanced galvanic microencapsulation (GME) in a ball mill with steel ball media. Miner. Eng. 143, 105931.
Senoro, D.B., Bonifacio, P.B., Mascarenas, D.R., Tabelin, C.B., Ney, F.P., Lamac, M.R.L., Tan, F.J., 2020. Spatial distribution of agricultural yields with elevated metal concentration of the island exposed to acid mine drainage. J. Degraded Min. Lands Manag. 8 (2), 2551–2558.
Silwamba, M., Ito, M., Hiroyoshi, N., Tabelin, C.B., Fukushima, T., Park, I., Jeon, S., Igarashi, T., Sato, T., Nyambe, I., Chirwa, M., 2020a. Detoxification of lead-bearing zinc plant leach residues from Kabwe, Zambia by coupled extraction-cementation method. J. Environ. Chem. Eng. 8 (4), 104197.
Silwamba, M., Ito, M., Hiroyoshi, N., Tabelin, C.B., Hashizume, R., Fukushima, T., Park, I., Jeon, S., Igarashi, T., Sato, T., Chirwa, M., 2020b. Recovery of lead and zinc from zinc plant leach residues by concurrent dissolution-cementation using zero-valent aluminum in chloride medium. Metals 10 (4), 531.
Singhi, B., Laskar, A.I., Ahmed, M.A., 2016. Investigation on soil-geopolymer with slag, fly ash and their blending. Arabian J. Sci. Eng. 41, 393–400.
Tabelin, C.B., Igarashi, T., 2009. Mechanisms of arsenic and lead release from hydrothermally altered rock. J. Hazard Mater. 169, 980–990.
Tabelin, C.B., Igarashi, T., Tamoto, S., 2010. Factors affecting arsenic mobility from hydrothermally altered rock in impoundment-type in situ experiments. Miner. Eng. 23, 238–248.
Tabelin, C.B., Igarashi, T., Tamoto, S., Takahashi, R., 2012a. The roles of pyrite and calcite in the mobilization of arsenic and lead from hydrothermally altered rocks excavated in Hokkaido, Japan. J. Geochem. Explor. 119–120, 17–31.
Tabelin, C.B., Basri, A.H.M., Igarashi, T., Yoneda, T., 2012b. Removal of arsenic, boron, and selenium from excavated rocks by consecutive washing. Water, Air, Soil Pollut. 223, 4153–4167.
Tabelin, C.B., Igarashi, T., Yoneda, T., 2012c. Mobilization and speciation of arsenic from hydrothermally altered rock containing calcite and pyrite under anoxic conditions. Appl. Geochem. 27, 2300–2314.
Tabelin, C.B., Igarashi, T., Takahashi, R., 2012d. Mobilization and speciation of arsenic from hydrothermally altered rock in laboratory column experiments under ambient conditions. Appl. Geochem. 27, 326–342.
Tabelin, C.B., Igarashi, T., Yoneda, T., Tamamura, S., 2013. Utilization of natural and artificial adsorbents in the mitigation of arsenic leached from hydrothermally altered rock. Eng. Geol. 156, 58–67.
Tabelin, C.B., Hashimoto, A., Igarashi, T., Yoneda, T., 2014a. Leaching of boron, arsenic and selenium from sedimentary rocks: I. Effects of contact time, mixing speed and liquid-to-solid ratio. Sci. Total Environ. 472, 620–629.
Tabelin, C.B., Hashimoto, A., Igarashi, T., Yoneda, T., 2014b. Leaching of boron, arsenic and selenium from sedimentary rocks: II. pH dependence, speciation and mechanisms of release. Sci. Total Environ. 473, 244–253.
Tabelin, C.B., Veerawattananun, S., Ito, M., Hiroyoshi, N., Igarashi, T., 2017a. Pyrite oxidation in the presence of hematite and alumina: II. Effects on the cathodic and anodic half-cell reactions. Sci. Total Environ. 581–582, 126–135.
Tabelin, C.B., Sasaki, R., Igarashi, T., Park, I., Tamoto, S., Arima, T., Ito, M., Hiroyoshi, N., 2017b. Simultaneous leaching of arsenite, arsenate, selenite and selenate, and their migration in tunnel-excavated sedimentary rocks: II. Kinetic and reactive transport modeling. Chemosphere 188, 444–454.
Tabelin, C.B., Veerawattananun, S., Ito, M., Hiroyoshi, N., Igarashi, T., 2017c. Pyrite oxidation in the presence of hematite and alumina: I. Batch leaching experiments and kinetic modeling calculations. Sci. Total Environ. 580, 687–689.
Tabelin, C.B., Sasaki, R., Igarashi, T., Park, I., Tamoto, S., Arima, T., Ito, M., Hiroyoshi, N., 2017d. Simultaneous leaching of arsenite, arsenate, selenite and selenate, and their migration in tunnel-excavated sedimentary rocks: I. Column experiments under intermittent and unsaturated flow. Chemosphere 186, 558–569.
Tabelin, C.B., Igarashi, T., Villacorte-Tabelin, M., Park, I., Opiso, E.M., Ito, M., Hiroyoshi, N., 2018. Arsenic, selenium, boron, lead, cadmium, copper, and zinc in naturally contaminated rocks: a review of their sources, modes of enrichment, mechanisms of release, and mitigation strategies. Sci. Total Environ. 645, 1522–1553.
Tabelin, C.B., Corpuz, R.D., Igarashi, T., Villacorte-Tabelin, M., Ito, M., Hiroyoshi, N., 2019. Hematite-catalysed scorodite formation as a novel arsenic immobilisation strategy under ambient conditions. Chemosphere 233, 946–953.
Tabelin, C.B., Silwamba, M., Paglinawan, F.C., Mondejar, A.J.S., Duc, H.G., Resabal, V.J., Opiso, E.M., Igarashi, T., Tomiyama, S., Ito, M., Hiroyoshi, N., 2020a. Solid-phase partitioning and release-retention mechanisms of copper, lead, zinc and arsenic in soils impacted by artisanal and small-scale gold mining (ASGM) activities. Chemosphere 260, 127574.
Tabelin, C.B., Corpuz, R.D., Igarashi, T., Villacorte-Tabelin, M., Alorro, R.D., Yoo, K., Raval, S., Ito, M., Hiroyoshi, N., 2020b. Acid mine drainage formation and arsenic mobility under strongly acidic conditions: importance of soluble phases, iron oxyhydroxides/oxides and nature of oxidation layer on pyrite. J. Hazard Mater. 399, 122844.
Tabelin, C.B., Dallas, J., Casanova, S., Pelech, T., Bournival, G., Saydam, S., Canbulat, I., 2021. Towards a low-carbon society: a review of lithium resource availability, challenges and innovations in mining, extraction and recycling, and future perspectives. Miner. Eng. 163, 106743.
Tamoto, S., Tabelin, C.B., Igarashi, T., Ito, M., Hiroyoshi, N., 2015. Short and long term release mechanisms of arsenic, selenium and boron from a tunnel-excavated sedimentary rock under in situ conditions. J. Contam. Hydrol. 175, 60–71.
Tatsuhara, T., Arima, T., Igarashi, T., Tabelin, C.B., 2012. Combined neutralization–adsorption system for the disposal of hydrothermally altered excavated rock producing acidic leachate with hazardous elements. Eng. Geol. 139, 76–84.
Tigue, A., Malenab, R.A.J., Dungca, J.R., Yu, D.E.C., Promentilla, M.A.B., 2018. Chemical stability of one part geopolymer from soil and coal fly ash mixtures. Minerals 8, 411.
Tomiyama, S., Igarashi, T., Tabelin, C.B., Tangviroon, P., Ii, H., 2019. Acid mine drainage sources and hydrogeochemistry at the Yatani mine, Yamagata, Japan: a geochemical and isotopic study. J. Contam. Hydrol. 225, 103–502.
Veiga, M.M., Angeloci, G., Hitch, M., Colon Velasquez-Lopez, P., 2014. Processing centres in artisanal gold mining. J. Clean. Prod. 64, 535–544.
Velásquez-López, P.C., Veiga, M.M., Klein, B., Shandro, J.A., Hall, K., 2011. Cyanidation of mercury-rich tailings in artisanal and small-scale gold mining: identifying strategies to manage environmental risks in Southern Ecuador. J. Clean. Prod. 19 (9-10), 1125–1133.
Wang, L., Ji, B., Hu, Y., Liu, R., Sun, W., 2017. A review on in situ phytoremediation of mine tailings. Chemosphere 184, 594–600.
Williams, M., Apostol, A., Miguel, J., 1995. Mercury contamination in artisanal gold mining areas of eastern Mindanao, Philippines: a preliminary assessment. Technical Report WC/95/2/R, Overseas Geology Series. Br. Geol. Surv.
Wojdyr, M., 2010. Fityk: a general-purpose peak fitting program. J. Appl. Crystallogr. 43, 1126–1128.
Xu, H., Gong, W., Syltebo, L., Izzo, K., Lutze, W., Pegg, I.L., 2014. Effect of blast furnace slag grades on fly ash based geopolymer waste forms. Fuel 133, 332–340.
Yang, Y., Wei, Z., Chen, Y.L., Li, Y., Li, X., 2017. Utilizing phosphate mine tailings to produce ceramisite. Construct. Build. Mater. 155, 1081–1090.
Yuniati, M., Hijarima, T., Miki, H., Sasaki, K., 2015. Silicate covering layer on pyrite surface in the presence of silicon-cathecol complex for acid mine drainage prevention. Mater. Trans. 56, 1733–1741.
Zhao, X., Liu, C., Zuo, L., Wang, L., Zhu, Q., Wang, M., 2019. Investigation into the effect of calcium on the existence form of geopolymerized gel product of fly ash based geopolymers. Cement Concr. Compos. 103, 279–292.
Zielasek, V., Jürgens, B., Schulz, C., Biener, J., Biener, M.M., Hamza, A.V., Bäumer, M., 2006. Gold catalysts: nanoporous gold foams. Angew. Chem. Int. Ed. 45 (48), 8241–8244.
Zoleta, J.B., Itao, G.B., Resabal, V.J.T., Lubguban, A.A., Corpuz, R.D., Ito, M., Hiroyoshi, N., Tabelin, C.B., 2020. Improved pyrolysis behavior of ammonium polyphosphate-melamine-expandable (APP-MEL-EG) intumescent fire retardant coating system using ceria and dolomite as additives for I-beam steel application. Heliyon 6, e03119.